Lattice models for Josephson junctions and graphene superlattices

Ostroukh, V.

Chapter 1

Introduction

1.1 Preface

The topic of this thesis is the modeling of electronic devices on the nanometer scale. The need for such modeling appears because modern device engineering requires going to lower and lower length scales, where classical circuit dynamics does not work anymore. The first commercially available microprocessor from the early 1970's, the Intel 4004 processor, had a minimal feature size of 10 micrometers. In 2018 we are approaching one thousand times smaller minimal dimensions. This 10 nanometer length scale is still two orders of magnitude above the atomic limit, but comparable to the electron wave length. A quantum mechanical modeling, including the effects of quantum interference, is required to properly describe these devices.

Our focus is on lattice models, which describe how the electron dynamics is modified by the periodic potential of the atomic lattice. The modification can be dramatic, as in graphene, a carbon monolayer, where the conduction electrons move through the honeycomb lattice of carbon atoms as if they were massless relativistic particles. We explore what happens if the electrons are subject to an additional "superlattice" from a copper substrate.

Superconductivity is a macroscopic quantum effect, that is modified as well on the nanoscale. We consider the induced superconductivity in topological insulators, which have an insulating bulk but a conducting surface or edge. In one of these investigations we have collaborated with an experimental group in Delft, so that our modelling could be directly

applied to the measured data.

In the next subsections we introduce the topics that will play a central role in the following chapters of the thesis.

1.2 Josephson junctions

A Josephson junction is a weak link between two superconductors. A dissipationless supercurrent can flow through the junction and it can be controlled by application of a magnetic field. For that reason a Josephson junction is the basic circuit element in superconducting technology. Applications include sensitive magnetometers [1], single-electron transistors [2], quantum computers (in flux [3], charge [4], or phase [5] qubits), scanning probe microscopy [6], and metrology [7, 8].

Our interest in Josephson junctions is as a probe of current-carrying paths in the junction region. Different paths will include different amounts of magnetic flux, so a study of the magnetic field dependence of the supercurrent will provide information on where the current flows. This is of particular interest if the junction is formed out of a topological insulator, which is predicted to have a current flow confined to the edge of the material.

1.2.1 Josephson effect

Superconductors are characterized by a complex order parameter $\Delta = |\Delta|e^{i\phi}$. The amplitude gives the energy gap for single-particle excitations from the ground state [9]. The gap appears because an effective attraction between electrons (which can have a variety of origins) imparts an energy penalty for the appearance of an unpaired single electron. The phase of Δ plays no role in a single homogenous superconductor, but when there is a weak link, a phase difference can drive a supercurrent. This is the Josephson effect.

The Josephson effect has two manifestations, as a stationary effect (DC) and as a time-dependent effect (AC). We will be only concerned with the DC Josephson effect. This effect is fully characterized by the dependence of the free energy $F(\phi)$ on the superconducting phase difference ϕ across the junction. The derivative gives the supercurrent according to

$$I(\phi) = \frac{2e}{\hbar}\frac{dF}{d\phi}. \tag{1.1}$$

Because ϕ appears as a phase factor $e^{i\phi}$ in the order parameter, all physical properties must be 2π-periodic functions of ϕ. This includes the supercurrent, $I(\phi) = I(\phi + 2\pi)$.

A periodic function must have a maximum value, this is called the critical current $I_c = \max_\phi I(\phi)$. The ϕ dependence can be complicated at low temperatures, but at elevated temperatures all harmonics except the lowest one are suppressed, and we have the simple relation

$$I(\phi) = I_c \sin \phi. \tag{1.2}$$

The size of the critical current depends on the properties of the junction. If the weak link is formed by a point contact I_c is quantized in units of $e|\Delta|/\hbar$ [10].

1.2.2 Fraunhofer oscillations and Dynes-Fulton relation

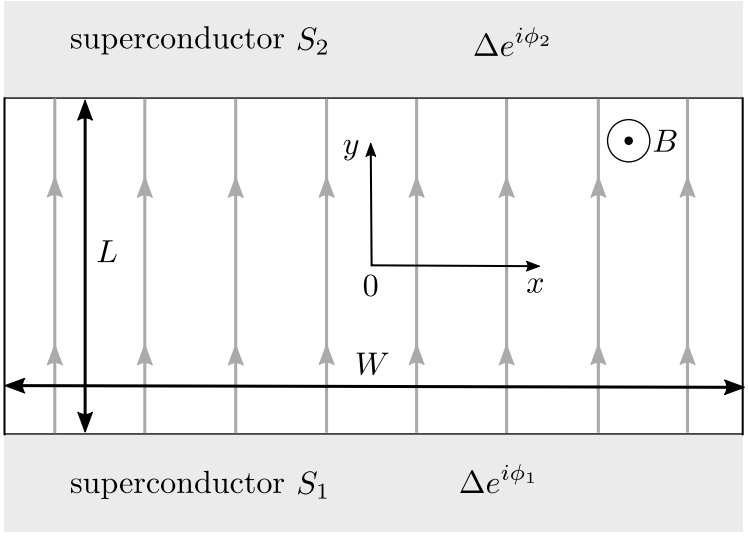

Figure 1.1. Schematic image of a Josephson junction. If the current is passing approximately along the y direction (grey arrows), the Dynes-Fulton analysis is applicable.

When a magnetic field B penetrates the junction region, the critical current depends on the enclosed flux in an oscillatory manner. These are called Fraunhofer oscillations, because the electron interference effect that gives rise to the oscillations is similar to the Fraunhofer diffraction pattern

in optics. We will use the Fraunhofer oscillations to find the current flow in the junction, and for that purpose we adopt a method developed by Dynes and Fulton [11].

We describe the method for a rectangular two-dimensional Josephson junction (se Fig. 1.1). Assume the existence of a local supercurrent density function $J(x, \phi)$, which is non-uniform because of some local inhomogeneities in the junction or, more interestingly, because of the edge states in a topological insulator. The magnetic-field dependence enters when we replace the phase ϕ by the gauge-invariant expression

$$\gamma(x) = \phi - \frac{2e}{\hbar} \int_{-L/2}^{L/2} A_y(x, y)\, dy = \phi - \frac{2e}{\hbar} BxL, \tag{1.3}$$

in the gauge $\mathbf{A} = (0, Bx, 0)$. The total current through the junction is

$$I(\phi, B) = \int_{-W/2}^{W/2} J(x, \phi - \frac{2e}{\hbar} BxL)\, dx. \tag{1.4}$$

We assume a sinusoidal current-phase relationship, $J(x, \phi) = J_c(x) \sin \phi$, with a spatially dependent critical current density $J_c(x)$. If the junction is $\pm x$ symmetric, so that $J_c(x)$ is an even function of x, we may decouple the coordinate and phase dependence,

$$I(\phi, B) = \left(\int_{-W/2}^{W/2} J_c(x) \cos\left(\frac{2e}{\hbar} BLx \right)\, dx \right) \sin \phi, \tag{1.5}$$

which leads to the critical current

$$I_c(B) = \left| \int_{-W/2}^{W/2} J_c(x) \cos\left(\frac{2e}{\hbar} BLx \right)\, dx \right|. \tag{1.6}$$

If $J_c(x)$ is uniform inside the junction, we recover the classical Fraunhofer pattern,

$$I_c(B) = I_c(0) \left| \frac{\sin(\pi\Phi/\Phi_0)}{\pi\Phi/\Phi_0} \right|, \tag{1.7}$$

where $\Phi = BWL$ is the total flux through the junction and $\Phi_0 = h/2e$ is the superconducting flux quantum. In contrast, if we have only edge currents, $J_c(x) = j_0 \left[\delta(x + W/2) + \delta(x - W/2)\right]$, we obtain an entirely different B-dependence,

$$I_c(B) = I_c(0) \left| \cos(\pi\Phi/\Phi_0) \right|, \tag{1.8}$$

characteristic of a SQUID (a superconducting quantum interference device).

More generally, the dependence $J_c(x)$ can be extracted from the measured $I_c(B)$ by a Fourier transformation,

$$J_c(x) = \frac{L}{\Phi_0} \int_{-\infty}^{\infty} \tilde{I}_c(B) \cos\left(2\pi BLx/\Phi_0\right) dB. \tag{1.9}$$

The tilde $\tilde{I}$ indicates that one should distinguish $+I_c$ from $-I_c$. In practice this means that one has to switch between + and − every time, when $I_c(B)$ touches zero.

The Dynes-Fulton analysis is simple and informative, but the basic assumption of a local supercurrent density function can give false results. In fact, Chapters 2, 3, and 4 describe situations where we must go beyond this approximation.

1.3 Graphene superlattices

Materials consisting of single-atom monolayers are actively studied for two main reasons: Firstly, due to effectively 2D physics, they often have unique physical properties. Secondly, they fit well into the modern electronics design, where elements are primarily located on a surface. For many decades it was assumed that monolayers are not thermodynamically stable, but would roll up as a scroll. We now know that this does not necessarily happen. Andre Geim and Konstantin Novoselov were awarded the 2010 Nobel Prize for their demonstration that carbon can form a stable monolayer, called graphene. The European Union research initiative "Graphene Flagship" [12] aims at bringing graphene and other 2D materials from scientific laboratories to industrial applications.

Our research has addressed a particular topic in this arena, the modification of graphene by a periodic potential imposed by a commensurate substrate, forming a "superlattice".

1.3.1 Electronic properties

Graphene has a honeycomb lattice consisting of two triangular sublattices. The unit cell has two atoms, labeled A and B. The tight-binding Hamiltonian is

$$H = -t \sum_{\langle i,j \rangle} (a_i^\dagger b_j + b_i^\dagger a_j), \tag{1.10}$$

with $\langle i, j \rangle$ indicating nearest neighbor atoms. The nearest-neighbor hopping amplitude is t, and a, b denote fermion annihilation operators on the A and B sublattice. Atoms on the same sublattice are not coupled by nearest-neighbor hopping.

The first Brillouin zone is a hexagon, with a band structure that has a conical singularity (a socalled Dirac point) at the corners of the hexagon. Near a corner the Hamiltonian can be linearized in momentum $\mathbf{k}$, resulting in the Dirac Hamiltonian

$$H = \hbar v_F \begin{pmatrix} 0 & k_x - ik_y \\ k_x + ik_y & 0 \end{pmatrix} = \hbar v_F (k_x \sigma_x + k_y \sigma_y). \tag{1.11}$$

This 2×2 matrix operator acts on a two-component wave function $\psi = (\psi_A, \psi_B)$, containing the wave amplitudes on the A and B sublattice. The Pauli matrices σ_x and σ_y are called "pseudospin" operators, because this sublattice degree of freedom is not a real spin. (The real spin plays no role in zero magnetic field.)

The energy spectrum of this Hamiltonian forms a Dirac cone,

$$E(\mathbf{k}) = \pm \hbar v_F |\mathbf{k}|. \tag{1.12}$$

The Fermi velocity $v_F = 3ta/2 \approx 10^6$ m/s plays the role of the speed of light in the relativistic Dirac equation for particles without mass. For this reason electrons in graphene are often referred as "massless". The Hamiltonian (1.11) has the property that the current operator

$$\mathbf{j} = \frac{\partial H}{\partial \mathbf{k}} = v_F \boldsymbol{\sigma} \tag{1.13}$$

locks the sublattice degree of freedom to the direction of propagation — one speaks of "pseudospin-momentum locking".

In particle physics there is the notion that massless electrons on a lattice must come in pairs, an effect known as "fermion-doubling". The same effect is operative in graphene: the two opposite corners of the hexagonal Brillouin zone, labeled K and K', are not related by a reciprocal lattice vector, so they are inequivalent "valleys" in the bandstructure. Each produces a massless Dirac fermion, described by the same Hamiltonian (1.11). The valley degree of freedom could be used to store information, and by analogy with electronics (information processing using the electron charge) and spintronics (spin-based information processing) one speaks of "valleytronics".

In this thesis we will propose a way to control the valley degree of freedom by means of a superlattice potential of the Kekulé type.

1.3.2 Kekulé-type superlattices

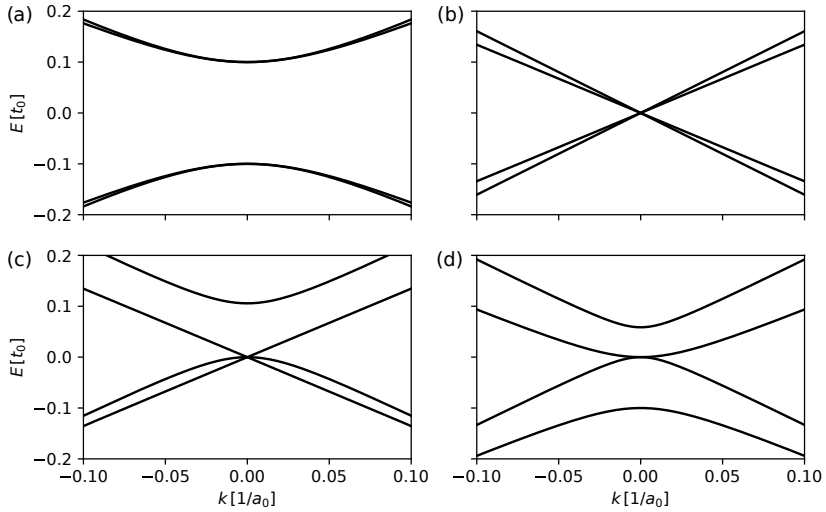

Figure 1.2. Four types of low-energy dispersion relations for the family of graphene superlattices with 6 atoms in the unit cell. The threefold enlargement of the unit cell (scaled by $\sqrt{3} \times \sqrt{3}$) folds the K and K' Dirac points onto the center of the Brillouin zone (the Γ point). Panels (a) and (b) correspond to a hopping amplitude modulation of Kekulé-O type (panel a) or Kekulé-Y type (panel b). Panels (c) and (d) correspond to a modulation of the atomic potential, resulting in a linear triple-point crossing (panel c) or a quadratic band crossing (panel d).

If graphene is deposited epitaxially on a substrate with the same honeycomb lattice, the dominant effect of the substrate is to couple the K and K' valleys of the Dirac fermions [13, 14]. The effect depends on whether the substrate predominantly modulates the hopping amplitudes or the atomic potentials. When the hopping amplitudes are modulated one speaks of a Kekulé-type superlattice. This name refers to the bond modulation in a benzene ring, studied by the chemist August Kekulé. Four different types of bandstructures in a graphene superlattice are shown in Fig. 1.2.

Our study of Kekulé-type graphene superlattices was motivated by an experiment performed by Gutierrez *et al.* [15], who realized a Y-shaped bond modulation by placing graphene on top of a copper substrate. That experiment was interpreted in terms of a gapped spectrum, as in panel

(a) of Fig. 1.2, however as we will show in Chapter 5, the spectrum remains gapless as in panel (b) — but with an unexpected valley-momentum locking.

1.4 Lattice models

Due to the rise of numerical computational power, numerical modeling on a lattice is one of the most important methods in modern science. Approximating a continuous differential or integral equation with a matrix analog on a space-time grid is a natural way to reformulate a problem for the machine, if analytical methods are not capable to solve it. Moreover, in practice often it happens also vice versa: numerical modeling can give some tips for actual way of solving the problem or point out interesting parameter regimes to explore.

Often lattice models also arise naturally from the system structure. First of all, this is an atomic-scale tight-binding model. Each atom is represented as a vertex on a graph, and interactions between them are bonds between these vertices. This graph can be mapped to the Hamiltonian matrix, if we know onsite energies for each vertex and hopping integrals for each bond [16]. These unknown values can be taken, for example, from density functional theory simulations, $k \cdot p$ perturbation theory, or from experiment. In general, lattice models are convenient to use whenever the system has some kind of sparse structure. This sparsity need not be obvious at first sight. For example, in Chapter 2 the sparse structure arises not from the microscopic but from the macroscopic properties of the device, namely, the existence of edge states.

1.4.1 Current calculations in tight-binding formalism

Experiments typically probe the system by measuring the electrical current, so that is the quantity we are most interested in when we perform a calculation. Here we briefly describe how the electrical current can be obtained from a lattice model.

We start with a general form of a many-body tight-binding Hamiltonian for non-interacting particles on a lattice:

$$H = -\sum_{i,j} H_{ij} c_i^\dagger(t) c_j(t). \tag{1.14}$$

This Hamiltonian naturally appears either from discretization of a continuous one (then usually square lattice is used), or from microscopic material structure (typical example of this is graphene, each lattice site then represents a real atom). We work in the Heisenberg representation where operators that do not commute with the Hamiltonian are time dependent.

Let us split our system into two arbitrary parts A and B and compute the current I_{BA} from part A to part B,

$$I_{BA} = \frac{dQ_B}{dt} = -e\left\langle \frac{dN_B}{dt} \right\rangle, \tag{1.15}$$

where $N_B(t) = \sum_{i\in B} c_i^\dagger(t)c_i(t)$ is a number operator of part B. Using the Heisenberg equation of motion and the fermionic commutation relations, we may rewrite this as

$$I_{BA} = \frac{ie}{\hbar}\langle [N_B, H]\rangle = \frac{ie}{\hbar}\left\langle \sum_{i\in B}\sum_{j\in A} H_{ij}c_i^\dagger(t)c_j(t) - H_{ji}c_j^\dagger(t)c_i(t) \right\rangle. \tag{1.16}$$

With the help of the lesser Green's function

$$G_{ij}^<(t,t') = \frac{i}{\hbar}\left\langle c_j^\dagger(t')c_i(t)\right\rangle,$$

this expression becomes

$$I_{BA} = e\sum_{i\in B}\sum_{j\in A}\left(H_{ij}G_{ji}^<(t,t) - H_{ji}G_{ij}^<(t,t)\right). \tag{1.17}$$

This expression is convenient for a computation in a tight-binding model, because it takes advantage from the sparsity of the Hamiltonian. We have to compute only those values of the Green's function, that correspond to hoppings which conect subsystems A and B. Usually the number of such sites is much less than the size of a system itself.

In equilibrium the Green's function depends only on the time difference

$$G_{ij}^<(t,t') = G_{ij}^<(t-t',0),$$

which means that we may replace $G_{ij}^<(t,t)$ in Eq. (1.17) with $G_{ij}^<(0,0)$. To compute it, we take a Fourier transform and switch to the frequency domain,

$$\begin{aligned} G_{ij}^<(\omega) &= \int_{-\infty}^{+\infty} G_{ij}^<(t,0)e^{i\omega t}dt, \\ G_{ij}^<(t,t') &= \frac{1}{2\pi}\int_{-\infty}^{+\infty} G_{ij}^<(\omega)e^{-i\omega(t-t')}d\omega. \end{aligned} \tag{1.18}$$

To compute these expressions, let us define the retarded and advanced Green's functions,

$$\begin{aligned} G^R_{ij}(t,t') &= -\frac{i}{\hbar}\Theta(t-t')\left\langle\left\{c_i(t), c_j^\dagger(t')\right\}\right\rangle, \\ G^A_{ij}(t,t') &= \frac{i}{\hbar}\Theta(t'-t)\left\langle\left\{c_i(t), c_j^\dagger(t')\right\}\right\rangle. \end{aligned} \tag{1.19}$$

As it is shown in [17], their Fourier transforms have a convenient form for numerical computation,

$$G^{R/A}_{ij}(\omega) = (\hbar\omega - H \pm i\eta)^{-1}. \tag{1.20}$$

which in a finite system requires a numerical inversion of the Hamiltonian. For an infinite system it needs to be modified by inclusion of the self-energy of the translation-invariant part of the system Σ^R or Σ^A, usually referred to as a "lead":

$$G^{R/A}_{ij}(\omega) = \left(\hbar\omega - H - \Sigma^{R/A} \pm i\eta\right)^{-1}. \tag{1.21}$$

In this thesis we make use of the Kwant toolbox [16], which implements the calculation of the Green's functions for arbitrary tight-binding Hamiltonians.

Once we have determined the Green's functions, we proceed as follows. In equilibrium one has [17, 18]

$$G^<_{ij}(\omega) = i f_0(\hbar\omega) A_{ij}(\omega), \tag{1.22}$$

where $f_0(\epsilon) = (\epsilon/k_BT + 1)^{-1}$ is the Fermi distribution function at energy ϵ and temperature T. The quantity $A_{ij}(\omega)$ is the socalled spectral density, defined by

$$A_{ij}(\omega) = i\left(G^R_{ij}(\omega) - G^A_{ij}(\omega)\right). \tag{1.23}$$

Using this relation, we may write the Green's function in Eq. (1.17) as

$$G^<_{ij}(0,0) = -\frac{1}{2\pi}\int_{-\infty}^{+\infty} f_0(\hbar\omega)\left(G^R_{ij}(\omega) - G^A_{ij}(\omega)\right)d\omega. \tag{1.24}$$

We can evaluate this integral by contour integration in the complex energy plane. The Fermi distribution function has poles at $\omega = i\omega_p$, where $\omega_p = (2p+1)\pi k_BT/\hbar$ for integer p is a fermionic Matsubara frequency. The retarded Green's function has poles only in lower half of the complex

plane, and the advanced Green's function only in the upper half. Closing the contour in the upper half of the complex plane for the retarded Green's function and in the lower half for the advanced Green's function, and evaluating the integrals by summing over the residues at the poles, we arrive at

$$G^{<}_{ij}(0,0) = i\frac{k_B T}{\hbar}\sum_{p=-\infty}^{+\infty} G^R_{ij}(i\omega_p). \tag{1.25}$$

Now we may insert this into Eq. (1.17) to obtain an equation for the equilibrium current,

$$\begin{aligned} I_{BA} &= i\frac{ek_B T}{\hbar}\sum_{p=-\infty}^{+\infty}\sum_{i\in B}\sum_{j\in A} H_{ij}G^R_{ji}(i\omega_p) - H_{ji}G^R_{ij}(i\omega_p) \\ &= 2\frac{ek_B T}{\hbar}\sum_{p=0}^{+\infty}\sum_{i\in B}\sum_{j\in A}\Im\left(H_{ji}G^R_{ij}(i\omega_p) - H_{ij}G^R_{ji}(i\omega_p)\right). \end{aligned} \tag{1.26}$$

This result forms the basis of our calculations of the supercurrent through a Josephson junction.

1.5 This thesis

Here we will give a brief overview of what will be explored in this thesis.

1.5.1 Chapter 2

Work, represented in this chapter, was motivated by V. S. Pribiag *et. al.* [19] (at that moment this paper was not yet published). Authors were performing superconducting quantum interference measurements in Josephson junctions, made with InAs/GaSb quantum wells. InAs/GaSb is a two-dimensional topological insulator [20, 21], therefore we expect existence of helical quantum spin Hall edge modes in the regime, when Fermi energy is inside the topological gap. This means, that SNS junction can be driven by gate from bulk-dominated regime to edge dominated (when the transport happens through the helical modes, and bulk is gapped). This transition was indeed observed in the SQI measurements, alongside with more peculiar phenomenon, displayed on the Fig. 1.3.

In the edge-dominated regime, in addition to expected SQUID-like dependency of switching current on transversal magnetic field (series of

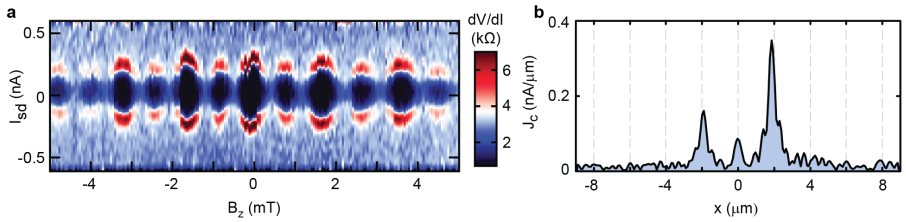

Figure 1.3. (a) Quantum interference pattern in Josephson junction with edge-dominated transport through normal part, that demonstrates $2\Phi_0$ periodicity in SQUID-like Josephson junction instead of expected Φ_0. Taken from Ref. [19]. (b) Current profile through the bulk of the junction, assuming validity of Dynes-Fulton analysis [11]. This picture was our original motivation for the research, represented in Chapter 2. Reprinted by permission from Springer Customer Service Centre GmbH: Springer Nature, Nature Nanotechnology, V. S. Pribiag, A. J. A. Beukman, F. Qu, M. C. Cassidy, C. Charpentier *et al.*, "Edge-mode superconductivity in a two-dimensional topological insulator", Nature Nanotech. **10**, 593–597 (2015), Copyright 2015.

equally spaced peaks of equal height with period of Φ_0/A, where A is area of Josephson junction and $\Phi_0 = h/2e$ is a superconducting flux quantum), authors observed a modulation between peaks amplitude, usually referred to as even-odd effect or $2\Phi_0$-periodicity. This could be explained by the fermion-parity anomaly [22], but would require quasiparticle poisoning time of order of tens of seconds [23], therefore it was extremely unlikely. Other possibility would be an existence of a conducting channel in the middle of SNS junction, but this requires fine-tuning and improbable to occur in different devices, which happened in the experiments.

In this chapter we build a phenomenological model, that assumes existence of scattering between opposite quantum spin Hall edges along the NS interfaces, that is formed due to the influence of superconductor, locally pushing the Fermi level from the topological gap to conduction band. This opens several paths for even-odd beating in critical current to occur (see Fig. 2.1). To describe the effect quantitatively, we build a network model of quantum spin Hall Josephson junction and explore the relative amplitude of even-odd beating versus coupling strength between helical edge channel and non-helical channel near the NS interface of the junction.

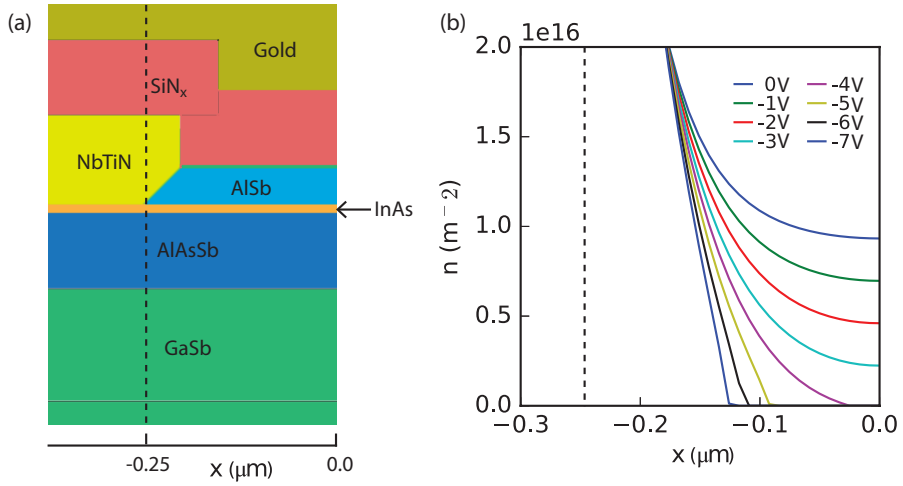

Figure 1.4. Schematic image of NS contact in experiment from Chapter 3. (a) Geometry of NS contact, that leads to the formation of a conducting channel along it, that enables transport between InAs edge channels. As it is shown in Chapter 2, this can lead to even-odd beating on top of SQUID-like quantum interference pattern. (b) Results of electrostatic simulations, that are performed using a finite element Poisson solver, based on this geometry. The electron density profile is changing as the top and bottom gate voltages are swept. The top gate voltage is indicated in the legend. In the lower gate voltage traces the electrons in the bulk are depleted while there is still a large electron density in the vicinity of the contacts. For clarification, the x-axis value where the NbTiN contact is on top of the InAs is indicated by the dashed line in both (a) and (b). The top gate is screened close to the contacts due to the triangular shape of the top AlSb barrier. Reprinted with permission from F. K. de Vries, T. Timmerman, V. P. Ostroukh, J. van Veen *et. al.*, Phys. Rev. Lett. **120**, 047702 (2018). Copyright 2018 by the American Physical Society.

1.5.2 Chapter 3

This chapter naturally continues the work from Chapter 2. At that moment it was already clarified, that alongside with topological edge channels, InAs/GaSb can host also trivial ones due to Fermi level pinning. Here we focus on superconducting transport through these trivial edges. Similarly to the previous chapter, we explore SNS junction, using superconducting quantum interference measurements and varying chemical potential in the normal part using top and bottom gates. Again, in the edge-conducting regime even-odd beating is observed.

On the experimental side of this chapter we describe in details experiments performed and obtained results. From the theoretical side (which was mainly the area of responsibility of author of this Thesis), we build a tight-binding model of the system, reproduce experimental data and demonstrate, that even-odd beating originates most probably from the conducting channel along the NS interface of the Josephson junction.

1.5.3 Chapter 4

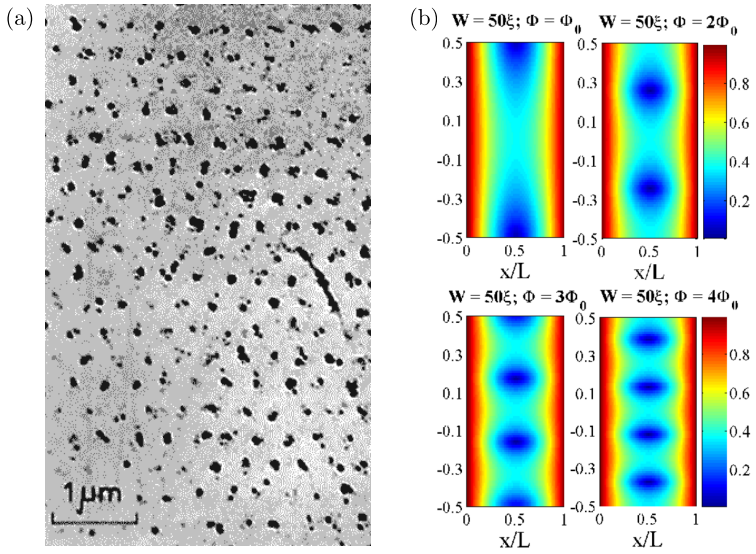

Figure 1.5. (a) Historically first observation of Abrikosov lattice from the experiment of Essman and Träuble [24]. Each black dot is a cobalt particle, bound to vortex core. Reprinted from U. Essmann and H. Träuble, "The direct observation of individual flux lines in type II superconductors", Physics Letters A **24**, 526–527 (1967), Copyright 1967, with permission from Elsevier. (b) Josephson vortex line formation in diffusive Josephson junctions, with increasing magnetic flux Φ, that penetrates normal part of the junction. Simulations by Cuevas and Bergeret [25]. Colorscale corresponds to the pair correlation function amplitude (which is effectively density of Cooper pairs), each minimum corresponds to the Josephson vortex core. Reprinted figure with permission from J. C. Cuevas and F. S. Bergeret, Phys. Rev. Lett. **99**, 217002 (2007). Copyright 2007 by the American Physical Society.

Vortices in superconductors are known already for a while and is still a subject of investigations. For example, Abrikosov [26] proposed a vortex

lattice in type-II superconductors to explain critical field scaling near the critical temperature (for type-II superconductors $H_c \propto T_c - T$, instead of $H_c \propto \sqrt{T_c - T}$ for type-I superconductors). Each Abrikosov vortex carries magnetic flux Φ_0, usually they organize into triangular lattice for magnetic field higher than first critical, or can be pinned to defects in the bulk [9]. Correct description of thermodynamical or transport properties of type-II superconductors is impossible without taking them into account.

Another superconducting setup, where one can find vortices, is a Josephson junction. Its two NS interfaces act as two reflecting surfaces in Fabry-Pérot interferometer, and interference in this setup leads to the destruction of current in several points along the 1D line in the normal part. [9]. These points are cores of so-called Josephson vortices. Contrary to Abrikosov vortices, they carry not quantized flux and generally appear in vortex-antivortex pairs. They are also responsible for the formation of Fraunhofer oscillations of critical current in magnetic field in the case of short wide Josephson junction:

$$I_c(\Phi) = I_{c0}\frac{\sin(\pi\Phi/\Phi_0)}{\Phi/\Phi_0}, \tag{1.27}$$

where $\Phi = BWL$ is a magnetic flux, penetrating to the junction area, and $\Phi_0 = h/2e$ is a superconducting flux quantum. However, cases, when then arrange to 2D structure instead of 1D chain, were unknown.

In this chapter we point out, that in the case of warped Fermi surface is is possible also to achieve two-dimensional Josephson vortex lattice. This happens, because current carriers receive preferred direction of motion, that drastically changes interference pattern inside a junction. We illustrate this finding using semiclassical description and a tight-binding model, both independently leading to the consistent picture. Also we explore, how this vortex lattice and edge effects impact $I_c(B)$ dependency of a junction and figure out, that it plays important role in high-B asymptotic behavior of critical current decay.

1.5.4 Chapter 5

Graphene offers a rich platform for wide range of applications in nanoelectronics. Conduction electrons in graphene have three distinct spin-like quantum numbers: spin itself, sublattice pseudospin and valley isospin. One of goals in graphene research is to provide handles for controlling these degrees of freedom. Another important quest is opening controllable gap

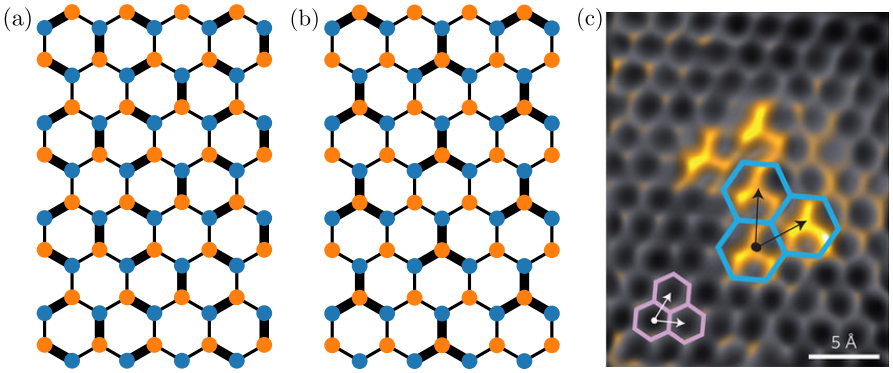

Figure 1.6. (a) Kek-O bond density modulation, that couples valleys in graphene spectrum and opens a gap [27]. (b) Kek-Y bond density modulation, that couples valleys in grapene spectrum and removes their degeneracy without opening a gap, but inducing different velocities (Chapter 5). (c) An STM image from, that demonstrates Kek-Y bond density modulation in graphene on top of copper substrate [15]. Reprinted by permission from Springer Customer Service Centre GmbH: Springer Nature, Nature Physics, C. Gutiérrez, C.-J. Kim, L. Brown, T. Schiros, D. Nordlund *et al.*, "Imaging chiral symmetry breaking from Kekulé bond order in graphene", Nature Phys. **12**, 950 (2016), Copyright 2016.

in graphene spectrum, that will turn it into a semiconductor. That was the motivation of Cristopher Gutierrez *et. al.* [15], who tried to realize proposal [28] and open a gap by special bond density modulation (see Fig. 1.6(a)). They successfully induced the superlattice, placing graphene on top of Cu-111 substrate, but the bond modulation was different from one expected (Fig. 1.6(b, c)).

In this chapter we investigate this type of graphene-based superlattice. We demonstrate, that this type of modulation removes degeneracy between two Dirac cones of graphene spectrum, leaving the spectrum non-gapped. These Dirac cones are still symmetry-protected, as well as zeroth Landau level, that stays at zero energy with a double degeneracy, while all other Landau level get split. This is remarkably different from the expectations and opens a way to control valley degree of freedom in transport experiments in graphene or its analogues in optics or acoustics.